

Energy dispersive X-ray diffraction of lithium–silver vanadium phosphorous oxide cells: *in situ* cathode depth profiling of an electrochemical reduction–displacement reaction

Cite this: *Energy Environ. Sci.*, 2013, **6**, 1465

Received 15th January 2013
Accepted 5th March 2013

DOI: 10.1039/c3ee40152a

www.rsc.org/ees

Esther S. Takeuchi,^{*abc} Amy C. Marschilok,^{*ab} Kenneth J. Takeuchi,^{*a}
Alexander Ignatov,^d Zhong Zhong^e and Mark Croft^{*de}

Li/Ag₂VO₂PO₄ cells exhibit high power output and a 15 000 fold decrease in impedance upon initial discharge. Energy dispersive X-ray diffraction (EDXRD) allows dimensional resolution of the reaction progress *in situ*, revealing that silver metal (Ag⁰) initially forms at the electrode–electrolyte interface. This report contains the first description of an *in situ* EDXRD analysis of a cathode located within an intact Li-anode cell.

Materials containing vanadium centers have been of significant interest due to the opportunity for multiple electron transfer leading to high energy density. In large part due to the variable formal oxidation states (II–V) of vanadium cations, these materials display a rich electrochemistry.^{1,2} The vanadium bronze silver vanadium oxide, Ag₂V₄O₁₁, serves as an example of a vanadium based system that has demonstrated long term commercial success as the predominant battery cathode material powering implantable cardiac defibrillators.^{3–6} Another class of energy storage materials that have attracted significant attention are phosphates due to their chemical and thermal stability.⁷ However, the inherently low conductivity of phosphates must be addressed in order to facilitate their use in high power applications.

We hypothesized that the electrical conductivity of a bimetallic phosphate material could be significantly enhanced by *in situ* formation of electrically conducting metal particles upon reduction of one of the metal ions in the bimetallic compound,

Broader context

Full understanding of the electrochemical processes taking place in batteries continues to be elusive due to the multiplicity and complex natures of the reactions associated with discharge and charge processes, and the difficulties of analytical interrogation of these reactions. A direct approach to the interrogation of the reactions taking place inside batteries is to employ *in situ* strategies. Unfortunately, *in situ* measurements are often hindered by diminution of signal due to the housing of an electrochemical cell or by the need to create special housings that enable the measurement. We present here an energy dispersive X-ray diffraction (EDXRD) analysis powerful enough to penetrate steel housings and thus enable *in situ* study of lithium based cells. This report contains the first description of this technique being applied to a critical chemical reaction occurring within lithium anode cells. Further, in contrast to standard top down or transmission mode XRD methods which probe either the surface or the full sample thickness, the EDXRD technique allows interrogation of the electrode cross-section as a function of depth enabling identification of the chemical reaction front within the electrode.

addressing the conductivity limitations for poorly conducting phosphate based materials. Thus, we recently identified silver vanadium phosphorus oxides, Ag_wV_xP_yO_z as a material family of interest for next generation batteries, based on the desire to obtain the chemical stability observed in other phosphate cathode materials,⁸ achieve multiple electron transfer inherent in bimetallic materials, and provide the opportunity for the *in situ* generation of a conductive silver matrix.^{9,10}

Our hypothesis was confirmed as the Li/Ag₂VO₂PO₄ batteries demonstrated 205 mA h g⁻¹ to 2.0 V and 270 mA h g⁻¹ to 1.5 V under constant current discharge and supported 50 mA cm⁻² pulses above 1.5 V.¹¹ Further improvement in power capability was achieved *via* reduction of Ag₂VO₂PO₄ particle size.¹² The cell DC resistance values, AC impedance values and cathode electrical conductivity showed clear trends linked to the level of discharge.¹³ Most notably, the impact of reduction of Ag₂VO₂PO₄ of the cells was profound as a 15 000 fold decrease in impedance was observed with initial discharge.¹⁰ The decrease in impedance was concurrent with the formation of metallic Ag⁰ nanoparticles as observed by *ex situ* XRD and *ex situ* SEM.

^aDepartment of Chemistry, Stony Brook University, Stony Brook, NY 11794, USA. E-mail: esther.takeuchi@stonybrook.edu; amy.marschilok@stonybrook.edu; kenneth.takeuchi.1@stonybrook.edu

^bDepartment of Materials Science and Engineering, Stony Brook University, Stony Brook, NY 11794, USA

^cGlobal and Regional Solutions, Brookhaven National Laboratory, Upton, NY 11973, USA

^dDepartment of Physics and Astronomy, Rutgers University, Piscataway, NJ 08854, USA. E-mail: croft@physics.rutgers.edu

^eNational Synchrotron Light Source, Brookhaven National Laboratory, Upton, NY 11973, USA

While our mechanistic studies of the electrochemical reduction mechanism of $\text{Ag}_2\text{VO}_2\text{PO}_4$ reduction to date have utilized *ex situ* analyses, *in situ* techniques can provide additional insights regarding this battery system. *In situ* methods can allow direct interrogation of a battery electrode in its native environment, without exposure of the surfaces to ambient air, moisture, and other reactive and deleterious substances. Specifically, crystallographic *in situ* analysis of electroactive material can provide insight with the confidence that no structural change or decomposition occurred as a result of material removal from the cell or post-processing. While significant signal loss remains a challenge of *in situ* methods, it is possible to design specialized laboratory test cells which enable *in situ* measurements.^{14–19} However, these specialized designs often require use of non-standard battery materials (*i.e.* beryllium or Mylar windows, butyl rubber gaskets), atypical cell balance, construction, and geometry. The unique material and design requirements for the specialized *in situ* cells introduce new variables into the electrochemical experiment, and may result in data which are not fully representative of a typical battery.

EDXRD presents the first direct *in situ* method allowing interrogation of the $\text{Li}/\text{Ag}_2\text{VO}_2\text{PO}_4$ cell in its native environment. A synchrotron “wiggler” insertion device emits high energy radiation which can penetrate bulk engineering materials. EDXRD has been employed in the analysis of dense materials such as steel,^{20–25} and therefore can extend the benefits of *in situ* XRD beyond specialized cells to conventionally designed prototype and production level batteries. Recently, the unique attributes of EDXRD were exploited in the study of sodium metal halide cells operated at 300 °C where full size prototype type cells in steel casings were used in the analysis.²⁶

Another benefit of EDXRD in this embodiment is the ability to obtain a “tomographic” profile as a function of both depth of discharge and position within the electrode. In order to conduct the *ex situ* measurements discussed above, an entire cathode was recovered, ground into a fine powder, and used for analysis. As the entire cathode was used for the measurements, the data represent bulk measurements of average properties across the entire electrode. Thus, detailed insights of the electrochemical reduction progress as a function of location within the cathode were not available in the prior experiments.

The experimental cells used for the study reported here were standard coin type cells, using steel housings, lithium metal anodes, $\text{Ag}_2\text{VO}_2\text{PO}_4$ cathodes, and polymer membrane separators.^{11,12} Two $\text{Li}/\text{Ag}_2\text{VO}_2\text{PO}_4$ cells were examined where one cell was partially discharged by 1 electron equivalent or approximately 25% depth of discharge and a second cell was discharged to 4 electron equivalents or fully discharged. A representative discharge curve of $\text{Li}/\text{Ag}_2\text{VO}_2\text{PO}_4$ primary cells is shown (Fig. 1).

The energy dispersive X-ray diffraction (EDXRD) measurements in this work were performed at the Brookhaven National Synchrotron Light Source (NSLS) on the superconducting wiggler beam line X17B1.^{21–23,25} The substantial presence of Ag^0 (with its high atomic number and strong X-ray absorption) in the cathode, along with the long beam path through the entire

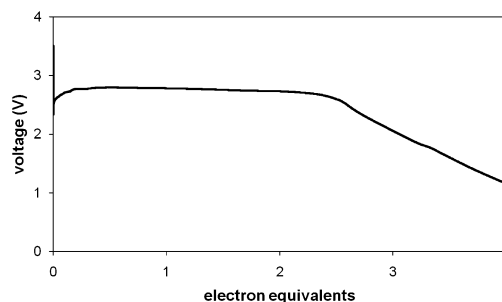


Fig. 1 Voltage curve of $\text{Li}/\text{Ag}_2\text{VO}_2\text{PO}_4$ electrochemical cell discharged under constant current at 0.15 mA cm^{-2} .

width of the cell, mandates the use of the high energies in these EDXRD measurements. The experimental setup involves “white beam” incident radiation with scattering at a fixed angle (2θ).^{21–23,25} The scattering angle (2θ) in this work was 3.05° . Additional details of the experimental setup, including transmission diffraction geometry and incident/scattered beam collimation slits have been previously described.^{22,23,25,26}

A high resolution Germanium detector measures the intensity *versus* energy of the scattered beam. The energies, E , of the scattered Bragg peaks are given by $E = b/[d_{hkl} \sin(\theta)]$ where d_{hkl} is the spacing associated with a specific interatomic plane labeled by the Miller indices (hkl). Here $b = hc/2$ where h is Planck’s constant, and c is the speed of light. In the conventional units, where d_{hkl} is measured in Å and E in keV, $b = 6.199 \text{ Å keV}$.

As in typical X-ray diffraction a chemical phase will exhibit a unique “fingerprint” pattern of Bragg reflections in its EDXRD spectrum. The relative intensity variations of these reflections can be used to profile the relative abundance of the respective chemical phases in an electrochemical cell as a function of location. For our purposes, comparison of the intensities of selected Bragg lines yields a satisfactory picture of the relative phase variations.

The intersection of the collimated incident and diffracted beam paths defines the gauge volume (GV) over which the crystalline scattering is averaged.^{22,23,25} The experiment was designed to generate a GV appropriate to the planar geometry of the coin cell (Fig. 2). When studying such planar systems, the long dimension of the GV (x -direction) is aligned parallel to the symmetry plane. The dimension of the GV in the profile direction (z -direction) is kept small for good profiling resolution. The

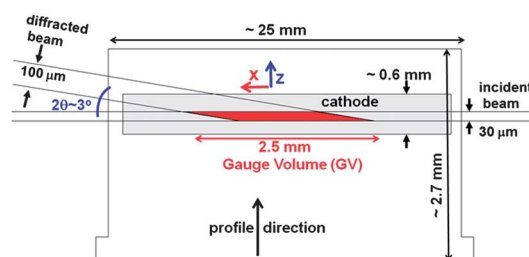


Fig. 2 A schematic of the coin cell with the diffraction geometry indicated for EDXRD.

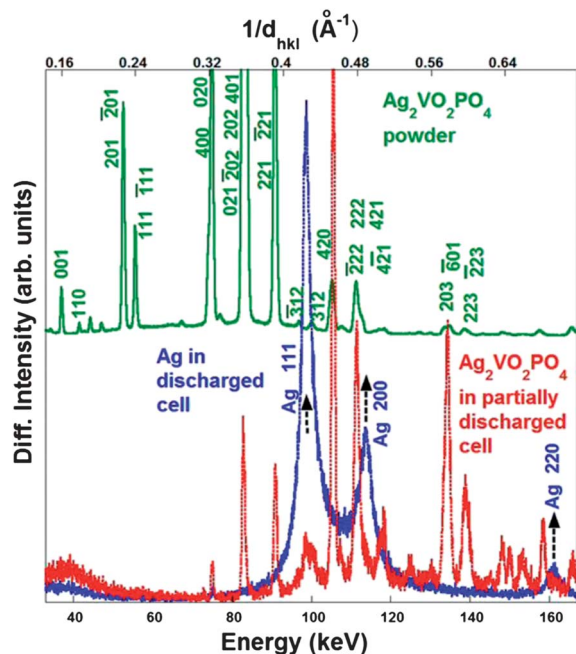


Fig. 3 EDXRD spectra of a $\text{Ag}_2\text{VO}_2\text{PO}_4$ powder standard (top), and selected cathode regions inside a fully discharged cell, manifesting a Ag-metal phase, and a pure $\text{Ag}_2\text{VO}_2\text{PO}_4$ phase region in a partially discharged cell (bottom). Here the partially discharged cell pattern is an average over 15 spectra to increase the signal to noise. Miller indices for $\text{Ag}_2\text{VO}_2\text{PO}_4$ and Ag metal are indicated.

other GV dimension parallel to the plane (y -direction) is enlarged to increase the scattered intensity signal. The incident beam is at a small angle ($2\theta = 3.05^\circ$). Along the incident beam (x -direction) the small angle leads to spreading of the GV into a flattened parallelogram.^{22,23} The GV dimensions are 2.5 mm in length (x -direction), 1 mm in width (y -direction), and 30 μm in height (z -direction).

Since we are using the diffraction spectra as the measure of the relative phase abundances in these electrochemical cells we begin with consideration of the relevant diffraction spectra (Fig. 3). The EDXRD reference spectrum of pure $\text{Ag}_2\text{VO}_2\text{PO}_4$ powder was collected and is shown in Fig. 3 (top). The calibrations of the energy and $1/d_{hkl}$ scales (along with the $2\theta = 3.05^\circ$ determination) were made using the Bragg and atomic fluorescence lines of a Pt-foil and CeO_2 powder standards. The Miller indices of the main peaks in the $\text{Ag}_2\text{VO}_2\text{PO}_4$ powder were determined by the excellent correspondence to the $1/d_{hkl}$ values determined from the JCPDF diffraction file (PDF#97-004-1947).

In the case of the fully discharged cell, the cathode diffraction patterns manifest an Ag-metal phase at all depths. The *in situ* fully discharged cell cathode spectrum, displayed in Fig. 3 (bottom) clearly manifests three Ag-metal Bragg peaks. The lines are broad with a non-Gaussian line shape. *Ex situ* XRD was also collected on fully and partially discharged $\text{Ag}_2\text{VO}_2\text{PO}_4$ material (Fig. 4). Only $\text{Ag}_2\text{VO}_2\text{PO}_4$ and Ag metal phases could be clearly discerned by XRD, both in the *ex situ* measurements and in the *in situ* EDXRD measurements. These findings are consistent with our prior *ex situ* diffraction studies which found Ag^0 nanoparticles to be formed in partially and fully discharged $\text{Ag}_2\text{VO}_2\text{PO}_4$ cells.^{10,12,13,27}

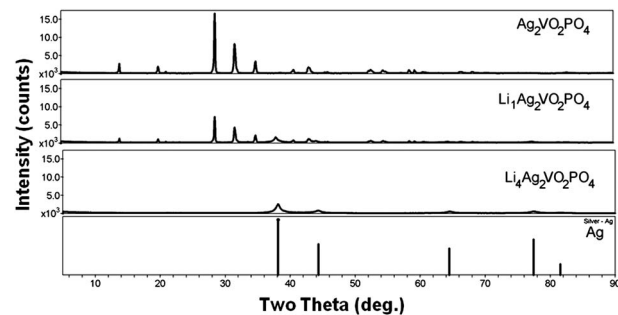


Fig. 4 *Ex situ* XRD spectra of as synthesized $\text{Ag}_2\text{VO}_2\text{PO}_4$, partially discharged ($\text{Li} = 1$), and fully discharged ($\text{Li} = 4$) $\text{Li}_x\text{Ag}_2\text{VO}_2\text{PO}_4$.

EDXRD spectra were collected *in situ* at selected points in the cathode of the fully discharged and partially discharged cells. It is useful to present a phase distribution profile in a 2-D contour plot format which allows comparison of multiple Bragg line intensities from multiple phases as a function of depth in an electrochemical cell.²⁶ Such plots are presented for the fully and partially discharged cells in this study (Fig. 5 and 6, respectively). Here the diffracted X-ray intensity appears in gray scale, the diffracted energy (E) is on the abscissa, and the depth in the cell, z , is on the ordinate. The fully discharged cell spectrum shows five Ag metal Bragg lines in the 80–200 keV range (Fig. 5). The diffraction pattern of the bcc steel cell body and external electrodes can also clearly be seen (Fig. 5 and 6). The diffraction contour profile of a partially discharged cell is shown (Fig. 6). Notably, in the partially discharged cell, the cathode layer furthest from the Li anode can be seen to be predominantly $\text{Ag}_2\text{VO}_2\text{PO}_4$, while the cathode layer closest to the Li anode shows the presence of Ag metal. In addition, a small amount of Ago formation is noted at the cathode/can interface. As the can is acting as the cathode current collector, formation of a

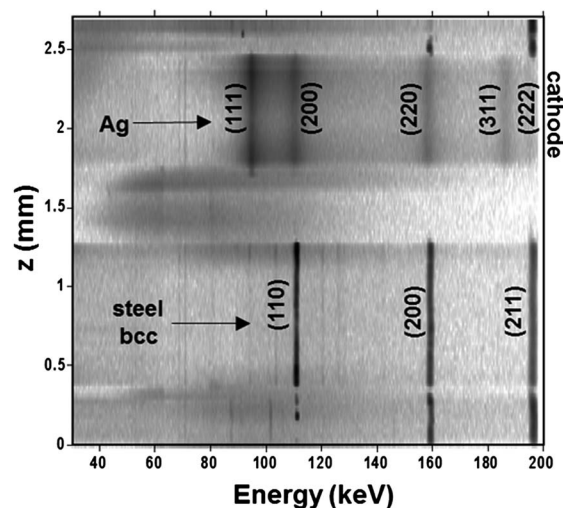


Fig. 5 Diffraction intensity contour plot of 90 diffraction patterns taken in equal increments through a 2.7 mm thick fully discharged cell. The horizontal axis corresponds to the diffracted X-ray energy, and the vertical axis is location, d , through the cell (with $z = 0$ being one cell external face). The Miller indices of silver (Ag) metal and the body centered cubic (bcc) steel cell body are indicated.

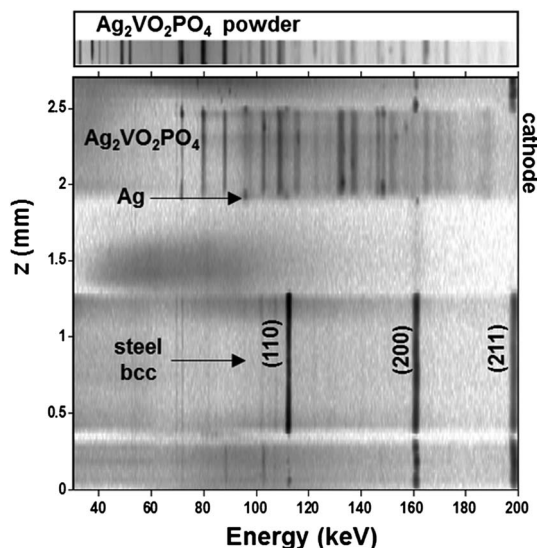


Fig. 6 Diffraction intensity contour plot of diffraction patterns taken in equal increments through a 2.8 mm thick partially discharged cell. In the upper insert the contour format diffraction pattern for $\text{Ag}_2\text{VO}_2\text{PO}_4$ is presented.

reduction product at that location is reasonable. In the case of the partially discharged cell, the correspondence between the Bragg lines for $\text{Ag}_2\text{VO}_2\text{PO}_4$ in the pure $\text{Ag}_2\text{VO}_2\text{PO}_4$ powder reference (presented as a contour plot in Fig. 6 top) and the partially discharged $\text{Li}/\text{Ag}_2\text{VO}_2\text{PO}_4$ cell is excellent above 70 keV. It is important to note however that the Bragg lines below 70 keV are totally suppressed for the *in situ* $\text{Ag}_2\text{VO}_2\text{PO}_4$ spectrum due to absorption.

In order to more precisely profile the cathode as a function of distance from the Li anode, a series of EDXRD spectra were acquired at 31 μm intervals in the partially discharged cell (Fig. 7). Here the spectra start in the Li-reservoir and proceeded into cathode (bottommost spectra up). The choice of $\Delta z = 0$ has been fixed as the nominal position where the leading edge of the GV first enters the cathode.

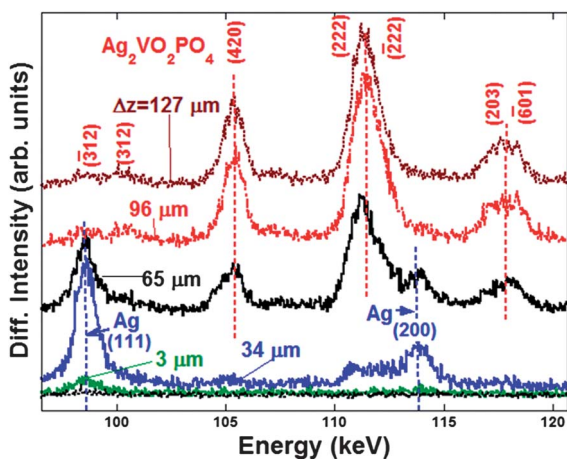


Fig. 7 A series of EDXRD spectra taken at 31 μm intervals entering and in the cathode of the partially discharged cell.

The bottommost spectrum, lying in the Li-reservoir, exhibits no Bragg lines. The first spectrum (3 μm) represents the first spectrum for which the GV has begun to enter the bottom portion of the cathode. The next spectrum (34 μm) shows the strongest Ag^0 phase signature along with the first indication that the furthest end of the GV has weakly penetrated some portion of the $\text{Ag}_2\text{VO}_2\text{PO}_4$ region of the cathode. The third spectrum (65 μm) evidences a clear coexistence between the two phases. Finally the fourth and fifth spectra (96 and 127 μm) are pure $\text{Ag}_2\text{VO}_2\text{PO}_4$ phase.

Thus, as one considers the cathode of a partially discharged cell beginning from the electrode–electrolyte interface adjacent to the Li anode, an Ag-metal phase is encountered first, an Ag-metal/ $\text{Ag}_2\text{VO}_2\text{PO}_4$ interface is encountered next and finally one passes into a pure $\text{Ag}_2\text{VO}_2\text{PO}_4$ phase. To chronicle this sequence the intensities of the Ag-(111) and $\text{Ag}_2\text{VO}_2\text{PO}_4$ -(420) Bragg lines can be used as semi quantitative indicators of their associated phase fraction variation with depth. Accordingly these peak intensities are plotted *versus* the Δz position in the cathode (Fig. 8).

In Fig. 8, the Ag^0 phase content rises rapidly between $\Delta z = 3$ and 34 μm , consistent with the crossing of the 30 μm long GV across a sharp interface between the Li-anode and the cathode. The signature of the Ag^0 phase decreases beyond $\Delta z \sim 40$ μm with an extrapolated disappearance at $\Delta z \sim 90$ μm . Concomitantly the $\text{Ag}_2\text{VO}_2\text{PO}_4$ phase appears very weakly at $\Delta z = 34$ μm and rises to saturation at and above $\Delta z \sim 90$ μm . The correlated Ag^0 -phase-content-decrease and $\text{Ag}_2\text{VO}_2\text{PO}_4$ -phase-content-increase indicate the passage through a reaction front between the two phases. The width of the reaction front appears broadened compared to the sharper, GV-limited spatial changes of the Ag^0 phase in the 3–34 μm range and to the steel cell–body interfaces. Circumstantially this is consistent with a rougher spatial structure in the reaction front. The total spatial extent of the Ag phase diffraction signal extends over ~ 90 μm . This 90 μm should roughly be the sum of the GV width (30 μm) and the intrinsic Ag phase layer width. Hence a rough estimate of the Ag^0 phase layer width is ~ 80 μm , approximately 13% of the cathode thickness. Upon reduction of the parent $\text{Ag}_2\text{VO}_2\text{PO}_4$, the reduction product or products other than silver metal, are not discernible by XRD as observed in both the *in situ* and *ex situ* experiments.

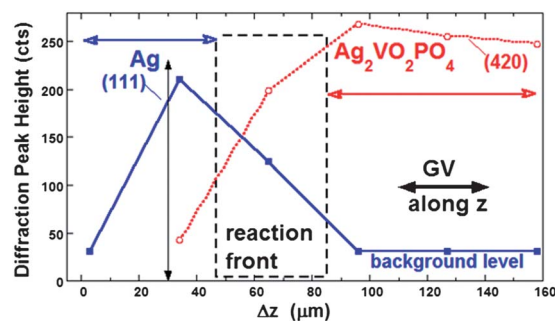
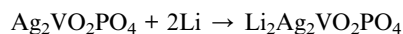
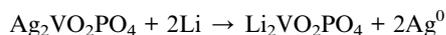


Fig. 8 Plots of the peak intensity of the Ag (111) and $\text{Ag}_2\text{VO}_2\text{PO}_4$ (420) Bragg lines as a function of depth (Δz) into the cathode of the partially discharged cell.

Due to the bimetallic nature of the cathode material, the discharge process for the cathode material can be considered as taking place in two reactions where there is reduction of silver and reduction of vanadium, as noted in the scheme below.



Assuming sequential progression of these two reactions, with $\text{Ag}^+ \rightarrow \text{Ag}^0$ reduction first, followed by $\text{V}^{5+} \rightarrow \text{V}^{3+}$ reduction, with 1 electron reduction, as in the partially discharged cell, only Ag^0 formation would be expected. If this were the case, 25% of the cathode thickness should show Ag^0 formation at 1 electron equivalent (25% depth of discharge). However, the EDXRD data (Fig. 7) shows Ag^0 formation up to only 13% of the cathode thickness, verifying that significant V^{n+} reduction must occur in parallel with the Ag^+ reduction through the initial stages of the reduction process. Notably, the fully discharged cell shows Ag^0 throughout the thickness of the cathode (Fig. 5), suggesting that complete Ag^+ to Ag^0 reduction is achieved during the discharge process.

The prior *ex situ* results support the findings of the *in situ* EDXRD. *Ex situ* XRD, a combination of *ex situ* V K-, V L-, Ag K-, and O K-edge X-ray absorption fine structure spectroscopy (XANES), and *ex situ* magnetic susceptibility measurements, indicated that on initial discharge, the predominant reaction is the reduction of silver ion to silver metal, and the reduction of vanadium takes place to some extent concurrently, but is the dominant reaction only after the reduction of the silver ion is complete.^{10,27}

Conclusions

The results presented above indicate that high-energy X-ray diffraction is an analytical approach that is capable of *in situ* “tomographic” profiling of the electrochemical phase changes in as assembled electrochemical cells. In contrast to standard top down or transmission mode XRD methods which probe either the surface or the full sample thickness, the EDXRD technique allows interrogation of the electrode cross-section as a function of depth enabling identification of the chemical reaction front within the electrode.

The formation of silver metal from the reduction of $\text{Ag}_2\text{VO}_2\text{PO}_4$ can be clearly seen at the electrode–electrolyte interface as well as the progression of the reduction reaction through the thickness of the cathode. This insight amplifies the point that full understanding of an electrochemical reaction in an active battery requires knowledge of the material status as a function of location within the cathode as well as the overall properties of the cathode material.

The resolution of the method reported here enabled identification of a reaction front in the 10's of microns. The current spatial resolution of the existing system at X17B1 should be capable of 5 micron resolution and it is believed that with modest improvements ~1 to 2 micron resolution should be possible. These phase profiling experiments on cathodes in coin

cells, when coupled with the previous work in much larger scale prototype cells suggest that a wide panoply of energy storage devices should be amenable to similar *in situ* characterization.

Acknowledgements

E. Takeuchi, A. Marschilok, and K. Takeuchi acknowledge support by the Department of Energy, Office of Basic Energy Sciences, under Grant DE-SC0008512. Utilization of the National Synchrotron Light Source (NSLS) was supported by US Department of Energy contract DE-AC02-76CH00016. The authors acknowledge Kevin Tanzil for assembly of the test cells.

Notes and references

- 1 E. S. Takeuchi, K. J. Takeuchi and A. C. Marschilok, in *Encyclopedia of Electrochemical Power Sources*, ed. J. Garche, C. Dyer, P. Moseley, Z. Ogumi, D. Rand and B. Scrosati, Elsevier, Amsterdam, 2009, vol. 4, pp. 100–110.
- 2 K. J. Takeuchi, A. C. Marschilok and E. S. Takeuchi, in *Vanadium: Chemistry, Biochemistry, Pharmacology and Practical Applications*, ed. A. S. Tracey, G. R. Willsky and E. S. Takeuchi, Taylor and Francis, New York, 2007, ch. 13.
- 3 K. J. Takeuchi, A. C. Marschilok, S. M. Davis, R. A. Leising and E. S. Takeuchi, *Coord. Chem. Rev.*, 2001, **219–221**, 283–310.
- 4 D. C. Bock, A. C. Marschilok, K. J. Takeuchi and E. S. Takeuchi, *Electrochim. Acta*, 2012, **84**, 155–164.
- 5 K. J. Takeuchi, R. A. Leising, M. J. Palazzo, A. C. Marschilok and E. S. Takeuchi, *J. Power Sources*, 2003, **119–121**, 973–978.
- 6 R. A. Leising, W. C. Thiebolt III and E. S. Takeuchi, *Inorg. Chem.*, 1994, **33**, 5733–5740.
- 7 N. Ilchev, Y. K. Chen, S. Okada and J. Yamaki, *J. Power Sources*, 2003, **119**, 749–754.
- 8 D. C. Bock, A. C. Marschilok, K. J. Takeuchi and E. S. Takeuchi, *J. Power Sources*, 2013, **231**, 219–225.
- 9 Y. J. Kim, C.-Y. Lee, A. C. Marschilok, K. J. Takeuchi and E. S. Takeuchi, *J. Power Sources*, 2011, **196**, 3325–3330.
- 10 E. S. Takeuchi, A. C. Marschilok, K. Tanzil, E. S. Kozarsky, S. Zhu and K. J. Takeuchi, *Chem. Mater.*, 2009, **21**, 4934–4939.
- 11 A. C. Marschilok, K. J. Takeuchi and E. S. Takeuchi, *Electrochem. Solid-State Lett.*, 2008, **12**, A5–A9.
- 12 Y. J. Kim, A. C. Marschilok, K. J. Takeuchi and E. S. Takeuchi, *J. Power Sources*, 2011, **196**, 6781–6787.
- 13 A. C. Marschilok, E. S. Kozarsky, K. Tanzil, S. Zhu, K. J. Takeuchi and E. S. Takeuchi, *J. Power Sources*, 2010, **195**, 6839–6846.
- 14 M. Morcrette, Y. Chabre, G. Vaughan, G. Amatucci, J.-B. Leriche, S. Patoux, C. Masquelier and J.-M. Tarascon, *Electrochim. Acta*, 2002, **47**, 3137–3149.
- 15 F. Ronci, B. Scrosati, V. R. Albertini and P. Perfetti, *Electrochem. Solid-State Lett.*, 2000, **3**, 174–177.
- 16 S. F. Amalraj and D. Aurbach, *J. Solid State Electrochem.*, 2011, **15**, 877–890.
- 17 A. Deb, U. Bergmann, E. J. Cairns and S. P. Cramer, *J. Synchrotron Radiat.*, 2004, **11**, 497–504.

- 18 A. Deb and E. J. Cairns, *Fluid Phase Equilib.*, 2006, **241**, 4–19.
- 19 K. Inoue, S. Fujieda, K. Shinoda, S. Suzuki and Y. Waseda, *Mater. Trans.*, 2010, **51**, 2220–2224.
- 20 A. Steuwer, J. R. Santisteban, M. Turski, P. J. Withers and T. Buslaps, *Nucl. Instrum. Methods Phys. Res., Sect. B*, 2005, **238**, 200–204.
- 21 M. C. Croft, N. M. Jisrawi, Z. Zhong, R. L. Holtz, K. Sadananda, J. R. Skaritka and T. Tsakalacos, *Int. J. Fatigue*, 2007, **29**, 1726–1736.
- 22 M. Croft, I. Zakharchenko, Z. Zhong, Y. Gurlak, J. Hastings, J. Hu, R. Holtz, M. DaSilva and T. Tsakalacos, *J. Appl. Phys.*, 2002, **92**, 578–586.
- 23 M. Croft, V. Shukla, E. K. Akdogan, N. Jisrawi, Z. Zhong, R. Sadangi, A. Ignatov, L. Balarinni, K. Horvath and T. Tsakalacos, *J. Appl. Phys.*, 2009, **105**.
- 24 M. Croft, Z. Zhong, N. Jisrawi, I. Zakharchenko, R. L. Holtz, J. Skaritka, T. Fast, K. Sadananda, M. Lakshmiopathy and T. Tsakalacos, *Int. J. Fatigue*, 2005, **27**, 1409–1419.
- 25 M. Croft, N. Jisrawi, Z. Zhong, K. Horvath, R. Holtz, M. Shepard, M. Lakshmiopathy, K. Sadanada, J. Skaritka, V. Shukla, R. K. Sadangi and T. Tsakalacos, *J. Eng. Mater. Technol.*, 2008, **130**, 021005.
- 26 J. Rijssenbeek, Y. Gao, Z. Zhong, M. Croft, N. Jisrawi, A. Ignatov and T. Tsakalacos, *J. Power Sources*, 2011, **196**, 2332–2339.
- 27 C. J. Patridge, C. Jaye, T. A. Abtew, B. Ravel, D. A. Fischer, A. C. Marschilok, P. Zhang, K. J. Takeuchi, E. S. Takeuchi and S. Banerjee, *J. Phys. Chem. C*, 2011, **115**, 14437–14447.